Ultrasonics Sonochemistry 20 (2013) 445–451

Contents lists available at SciVerse ScienceDirect

Ultrasonics Sonochemistry

journal homepage: www.elsevier.com/locate/ultson

Porous TiO_2 microspheres with tunable properties for photocatalytic air purification

Alberto Naldoni [a,*], Claudia L. Bianchi [b], Carlo Pirola [b], Kenneth S. Suslick [c]

[a] CNR-Istituto di Scienze e Tecnologie Molecolari, Via Golgi 19, 20133 Milano, Italy
[b] Dipartimento di Chimica, Università degli Studi di Milano, Via Venezian 21, 20133 Milano, Italy
[c] School of Chemical Science, University of Illinois at Urbana-Champaign, 600 S. Matthew Av., Urbana, IL 61801, USA

ARTICLE INFO

Article history:
Received 10 May 2012
Received in revised form 9 July 2012
Accepted 9 July 2012
Available online 20 July 2012

Keywords:
TiO_2
Nanostructured microsphere
Silica
Photocatalysis
NO_x

ABSTRACT

The synthesis of highly-crystalline porous TiO_2 microspheres is reported using ultrasonic spray pyrolysis (USP) in the presence of colloidal silica as a template. We have exploited the interactions between hot SiO_2 template particles surface and TiO_2 precursor that occur during reaction inside the droplets, to control the physical and chemical properties of the resulting particles. Varying the SiO_2 to titanium precursor molar ratio and the colloidal silica dimension, we obtained porous titania microspheres with tunable morphology, porosity, BET surface area, crystallite size, band-gap, and phase composition. In this regard, we have also observed the preferential formation of anatase vs. rutile with increasing initial surface area of the silica template. The porous TiO_2 microspheres were tested in the photocatalytic degradation of nitrogen oxides (NO_x) in the gas phase. USP prepared nanostructured titania samples were found to have significantly superior specific activity per surface area compared to a commercial reference sample (P25 by Evonik-Degussa).

1. Introduction

The synthesis of nanomaterials with desired morphologies and functionality remains a focus of intense current interest. Among the various morphologies explored (e.g., nanotubes, nanowires, nanorods, core–shell nanoparticles), hierarchically porous nanostructures have received substantial attention [1–6] not only for their unique or enhanced physicochemical properties, but also for their widespread potential applications, including uses for drug delivery, photonic materials, batteries and membrane fuel cells, and photocatalysis [7–15].

Titanium dioxide is a multifunctional material whose unusual electronic properties make it an especially important material for photoelectrochemical solar cell applications, hydrogen generation, and environmental remediation. Nanostructured TiO_2 exhibits superior photocatalytic activity compared to traditional bulk materials, and numerous strategies have been developed to synthesized hollow and porous TiO_2 nano/micro spheres [16–28]. Control over the physical and chemical properties of the resulting porous nanostructures, however, remains a scientific challenge.

As a synthetic tool, ultrasonic spray pyrolysis (USP) has several advantages over other traditional methods: production of micron- or submicron-sized spherical particles, high product purity, continuous operation, facile scale-up process from small to large production, and thorough control over chemical and physical compositions [21–23,29–48].

The oxides of nitrogen NO and NO_2 (NO_x) have a variety of negative impacts on human and environmental health ranging from serving as key precursors for the respiratory irritant ozone to forming nitric acid, which is a key component of acid rain. Hence it is of great interest to develop approaches that irreversibly remove NO_x from the atmosphere [49–54].

Here, we use USP as a phase-separated process for the synthesis of porous TiO_2 microspheres using colloidal silica nanoparticles as a template, and we examine their photocatalytic activity for the decomposition of NO_x.

The production of porous inorganic particles through the use of USP with a two-zone tube furnace has also been reported by Okuyama et al. Using pre-existing nanoparticles of silica [34–36] or titania (brookite [22], anatase [23] and Evonik-Degussa P25 [45], respectively) together with an organic template (such as polystyrene latex, PSL) to create porosity, they were able to synthesize spherical particles with controlled morphology and porosity. During evaporation of the solvent in the first heated zone, they observed a spontaneous self-organization of the PSL particles took place in the USP generated droplets. In the second heated zone, they burned away the organic template to produce porous SiO_2 or TiO_2 powder. The silica or titania particles' morphology and porosity could be controlled by changing the weight fraction of the PSL and the PSL particle diameter.

In order to design an efficient titania photocatalyst, it is also crucial obtaining the control over the physical properties, surface

* Corresponding author. Tel.: +39 02 503 14416; fax: +39 02 503 14405.
E-mail addresses: a.naldoni@iatm.cnr.it (A. Naldoni), claudia.bianchi@unimi.it (C.L. Bianchi), carlo.pirola@unimi.it (C. Pirola), ksuslick@illinois.edu (K.S. Suslick).

1350-4177/$ - see front matter © 2012 Elsevier B.V. All rights reserved.
http://dx.doi.org/10.1016/j.ultsonch.2012.07.003

chemical character, and chemical composition of the desired materials. In the present work, we report the USP of an aqueous solution of a commercially available titanium complex with colloidal SiO_2 nanoparticles as a porosity generating template to obtain porous titania microspheres with tunable properties. Exploiting the interactions at the interface between the silica surface and the titania precursor solution, we obtain control over the morphology, porosity, and physical and chemical properties (BET surface area, phase composition, band-gap, crystallite size, hydrophilicity *vs* hydrophobicity per unit surface area, photocatalytic activity per unit surface area) of the resulting porous titania materials.

2. Material and methods

2.1. Materials

All chemicals were handled in air and are available commercially. Silica colloid Ludox AS-30 (30 wt.% suspension in water; 12 nm diameter), titanium(IV) bis-(ammonium lactato) dihydroxide (50 wt.% water solution) were purchased from Aldrich Chemicals. Hydrofluoric acid (49 wt.%) was obtained from Acros Organics. Two SNOWTEX silica colloids (ST-XL: 35–50 nm, and ST-ZL: 70–100 nm) 40 wt.% water suspension were provided by Nissan Chemical Industries (Japan), while TiO_2 P25 was purchased from Evonik-Degussa (Germany). Water was purified and filtered using a Barnstead Nanopure system.

2.2. Synthesis

2.2.1. Porous TiO_2 microspheres

The precursor solution was composed by titanium(IV) bis-(ammonium lactato) dihydroxide (0.02 mol), purified water (50 mL, Barnstead Nanopure ion exchange) and colloidal silica variable in amount (Si:Ti molar ratio 1:1, 1:3 and 1:5) and particle size (12 nm, 35–50 nm, 70–100 nm). A piezoceramic transducer operating at 1.65 MHz was used to nebulize the starting solution through a polyethylene membrane into a glass apparatus. The mist was then carried by an air flow rate of 1 standard liter per minute (SLPM) into a furnace where the temperature was set at 1000 °C. After 8 h of collection into water-filled bubblers, the white colloidal particles were obtained by centrifugation at 9000×*g*. The products were washed with purified water three times and sampled for analysis.

2.2.2. Solid TiO_2 microspheres (T_USP)

Titanium dioxide solid spheres were synthesized using the same procedure as for porous titania microspheres but without adding colloidal silica as template.

2.2.3. Etching procedure

For all etched microspheres, removal of silica was done with HF 10 wt.% in water at room temperature. After 75 min., the particles were centrifuged and washed three times with purified water and once with 100% ethanol. After the etching, we obtained always about 350 mg of titania powder.

2.3. Characterization

Structural features of the prepared titanium dioxide microspheres have been determined by X-ray Powder Diffraction (XRPD) on a Siemens-Bruker D5000 diffractometer operating at 40 kV and 30 mA using a Cu Kα radiation source (λ = 1.5418 Å). In a typical experiment, a scan rate of 1°/min. and a step size of 0.05°. was used. All data was worked out using Jade X-ray analysis software package.

The powder morphology was observed with a JEOL 7000F field emission SEM operating at an acceleration voltage of 15 kV. Samples were prepared for analysis by the deposition of an absolute ethanol TiO_2 suspension on a silicon wafer, which was subsequently sputtered with a Pd–Au alloy.

TEM micrographs were taken using a JEOL 2100 Cryo microscope operating at 200 kV.

X-ray Photoelectron Spectroscopy (XPS) was performed by a M-Probe Instrument (SSI) equipped with a monochromatic Al K_α source (1486.6 eV) with a spot size of 200 × 750 μm and pass energy of 25 eV, providing a resolution for 0.74 eV. With a monochromatic source, an electron flood gun was used to compensate for the build-up of positive charge on the insulator samples during the analysis.

The surface area of materials was investigated by nitrogen adsorption studies using the Brunauer–Emmett–Teller (BET) method. Measurements have been performed using a Nova 2200e Surface Area and Pore Analyzer (Quantachrome Instruments) at liquid nitrogen temperature (−196 °C).

Diffuse reflectance spectra of the powders were measured on UV–vis spectrophotometer (PerkinElmer, Lambda 35), which was equipped with a diffuse reflectance accessory, as reported previously [58].

2.4. Photocatalytic testing

In the photocatalytic oxidation of nitrogen oxides (NO_x), immobilized particulate TiO_2 layers (ca. 50 mg) were prepared on glass sheets by deposition from a suspension of the samples in isopropanol [58]. The immobilized photocatalyst was placed into a Pyrex glass reactor (with a volume of 25 L) and irradiated with a halogen lamp (Jelosil, model HG500) emitting in the 340–400 nm wavelength range, with a nominal power of 500 W, at room temperature. The distance between the light source and the reactor was properly adjusted so that the UV irradiance at the sample surface is 10 ± 0.5 W/m^2. The relative humidity was kept constant in all runs (RH = 50%). Air, NO_x (NO = 10%, NO_2 = 90%), and N_2 gas streams were mixed to obtain the desired NO_x concentration (300 ppb) inside the photoreactor. The photodegradation products concentrations (NO and NO_2) were continuously monitored by an online chemiluminescent analyzer (Teledyne Instruments M200E). The NO_x adsorption onto the TiO_2 layer was determined through dark experiments.

3. Results and discussion

Nanostructured TiO_2 microspheres were prepared by USP employing a modification of the synthesis previously reported by Suslick et al. [21]. In this work, aiming to study the possibility to tailor physicochemical properties of TiO_2 microspheres we used a wider range of both SiO_2/TiO_2 molar ration and SiO_2 nanoparticles size [21]. In addition, a higher reaction temperature (1000 vs. 800 °C) was employed in order to study the role of SiO_2 in the anatase to rutile phase transition. An aqueous solution of a Ti^{IV} bis-(ammonium lactato) dihydroxide (which is air and water stable) containing colloidal silica was nebulized using a home-made ultrasonic generator (1.65 MHz) (cf. Section 2 for details). The resulting mist was carried into a furnace by an air flow and the SiO_2/TiO_2 nanocomposite microspheres so produced were collected in water-filled bubblers, isolated by centrifugation, and the silica template finally removed by etching with aqueous hydrogen fluoride (HF 10 wt.% in water). As a reference material, USP of the same aqueous solution of the Ti^{IV} complex without colloidal SiO_2 was performed, generating solid TiO_2 spheres (abbreviated T_USP; after etching with HF, abbreviated T_USP_HF).

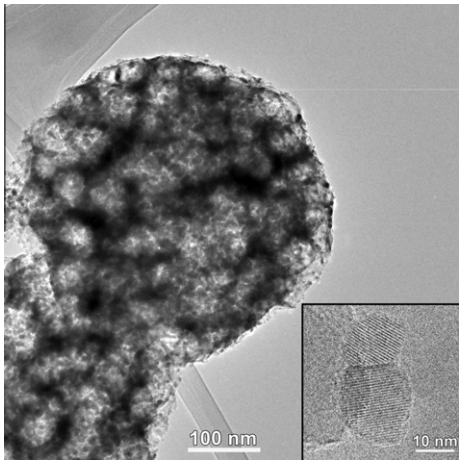

Fig. 1. Transmission electron micrograph of a USP-prepared porous TiO_2 microsphere (T13M); inset at higher magnification showing two 20 nm TiO_2 building blocks.

The porous nanostructure of USP particles was confirmed by TEM analysis (Fig. 1); abbreviations for microspheres prepared under various conditions are given in Table 1, together with their relevant properties. The titania microspheres were a few hundreds of nanometers in diameter; their nanostructure is built up of assembled individual nanoparticles between 20 and 40 nm in average size (Table 1). The inter-aggregations of these building blocks are due to condensation reactions among the hydroxyl groups on their surface [20], which results in the formation of the porous nanostructures.

Other authors have observed similar TiO_2 morphologies running the USP process with Ti^{IV} bis-(ammonium lactato) dihydroxide [21,57]. Nevertheless, in the present study we use a wider range of colloidal solid templates and a higher temperature (1000 vs 800 °C) than in previous published papers. The elevated temperature selected (1000 °C) shift the processes occurring inside a USP droplet to a shorter time scale. As a consequence, the solvent evaporation rate and the degree of supersaturation of the Ti precursor increase, which significantly affects the chemical and physical properties of USP products.

For example, we can control the morphology of our porous titania spheres by varying colloidal silica to titanium precursor molar ratio (Fig. 2). In addition, by using SiO_2 nanoparticles with different sizes (12, 35–50, 70–100 nm), we obtain porous TiO_2 spheres characterized by meso- or macroporosity (Fig. 3) [20]. The BET surface areas of the microspheres show a monotonic trend directly related to surface area of the template silica originally present (Table 1). If the silica content was too high (SiO_2/Ti = 1:1, SiO_2 size 12 or 35–50 nm), however, the superstructure was lost, presumably because of insufficient contact and binding among the TiO_2 nanoparticles (SI, Fig. S1).

For all samples, the microspheres' composition was confirmed by bulk elemental analysis, which showed only about 0.3 wt.% of Si left after etching. XPS analysis confirmed the absence of Si on the surface (SI, Fig. S2) and the presence of traces of surface fluorine (F/Ti $\leqslant$ 0.12 at./at.%) as fluoride (683.7 eV) [55] remaining from the etching step. The F/Ti ratio for the non-porous control sample T_USP_HF (see SI, Table S1) is much higher in comparison to the porous microspheres; this is probably because for the porous titania, HF selectively etched away the SiO_2 before attacking the remaining TiO_2, whereas for the non-porous titania, HF directly attacks the titania structure resulting in a higher remnant fluorine content.

There were no significant differences among samples in the XPS for the Ti *2p* region; the peak Ti $2p_{3/2}$ was regular and the binding energy (458.5 ± 0.1 eV) compared well with data for Ti^{IV} in TiO_2 (Ti_L, Fig. 4a and c) [56]. The only exception was observed for the non-porous T_USP microspheres, which present an additional species at 460.9 eV due to the unreacted precursor (Ti_P, Fig. 4c) [57], Ti^{IV} bis-(ammonium lactato) dihydroxide. Analysis of the oxygen peaks of porous TiO_2 microspheres showed, as often reported in the case of oxides, the presence of two components, attributed to lattice oxygen (O_L) in TiO_2 (529.6 eV), and to surface OH (O_{OH}) species (530.9 eV), respectively (Fig. 4b) [58]. The OH/O_{tot} surface ratio (SI, Table S1) correlates with the hydrophilicity of the TiO_2 surface, an important property affecting the samples photoactivity[56]. The values are all quite similar for the porous microspheres and for P25 (average OH/O_{tot} = 0.18), but the solid microspheres, T_USP and T_USP_HF, have a high ratio (OH/O_{tot} = 0.30 and 0.29, respectively) from excess oxygen originating from the unreacted precursor. Indeed, the deconvolution of the O *1s* peak reported in Fig. 4d clearly shows the presence of O_{OH}, O_L, and two additional oxygen species (O_P, $O_{OH'}$) that can be ascribed to the Ti^{IV} complex exploited in the USP synthesis. Interestingly, the computed values of OH/O_{tot} per unit surface area (SI, Table S2) increase with decreasing amounts of the initial SiO_2 template surface area.

USP process is substantially different from batch reactions in terms of the physicochemical interactions that occur during reaction. The USP process is unique in its continuous production of isolated sub-μm microreactors (i.e., each droplet formed by the

Table 1
BET Surface area, phase composition analysis*, anatase crystallite size, and band gap of solid and porous titania microspheres.

Sample	Si:Ti molar ratio	Silica size (nm)	Initial SiO_2 surf. area§ (m^2)	BET surf. area (m^2/g)	Anatase %	Anatase crystallite size† (nm)	Band gap (eV)
P25	–	–	0	49	75	25	3.17
T_USP	–	–	0	~1	36	41	2.92
T_USP_HF	–	–	0	~1	37	35	2.94
T15L	1:5	70–100	9	6	81	41	2.91
T15M	1:5	35–50	12	16	93	39	2.97
T15S	1:5	12	56	32	100	27	3.13
T13L	1:3	70–100	14	9	89	40	3.05
T13M	1:3	35–50	20	19	96	35	3.20
T13S	1:3	12	92	48	100	23	3.31
T11L	1:1	70–100	42	14	100	33	3.23
T11M	1:1	35–50	59	–	100	28	–
T11S	1:1	12	276	–	100	14	–

* Anatase % determined from XRPD:Anatase Ref. JCPDS 21–1272, Rutile Ref. JCPDS 21–1276.
§ For further details, see SI Fig. S3.
† Calculated by Sherrer's equation applied to the anatase (1 0 1) peak.

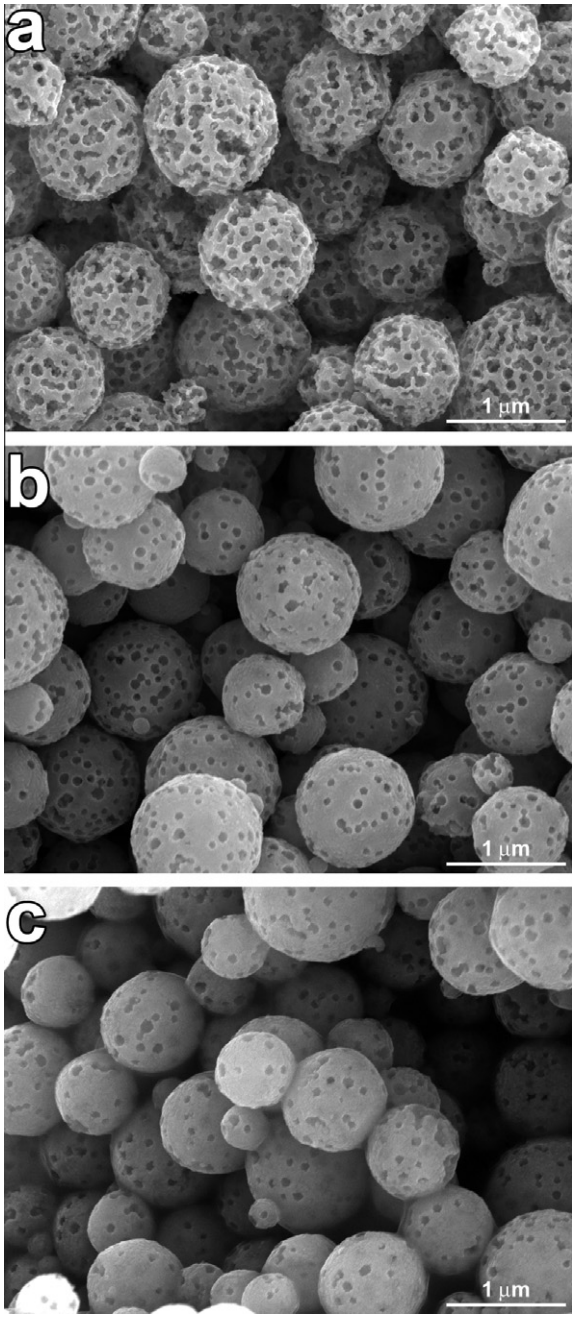

Fig. 2. Scanning electron micrographs (SEM) showing the effect of silica/titanium molar ratio on the particles' morphology. Sample abbreviations and SiO_2/Ti ratios are (a) T11L, 1:1; (b) T13L, 1:3; (c) T15L, 1:5; all with initial silica colloid template of 70–100 nm diameter.

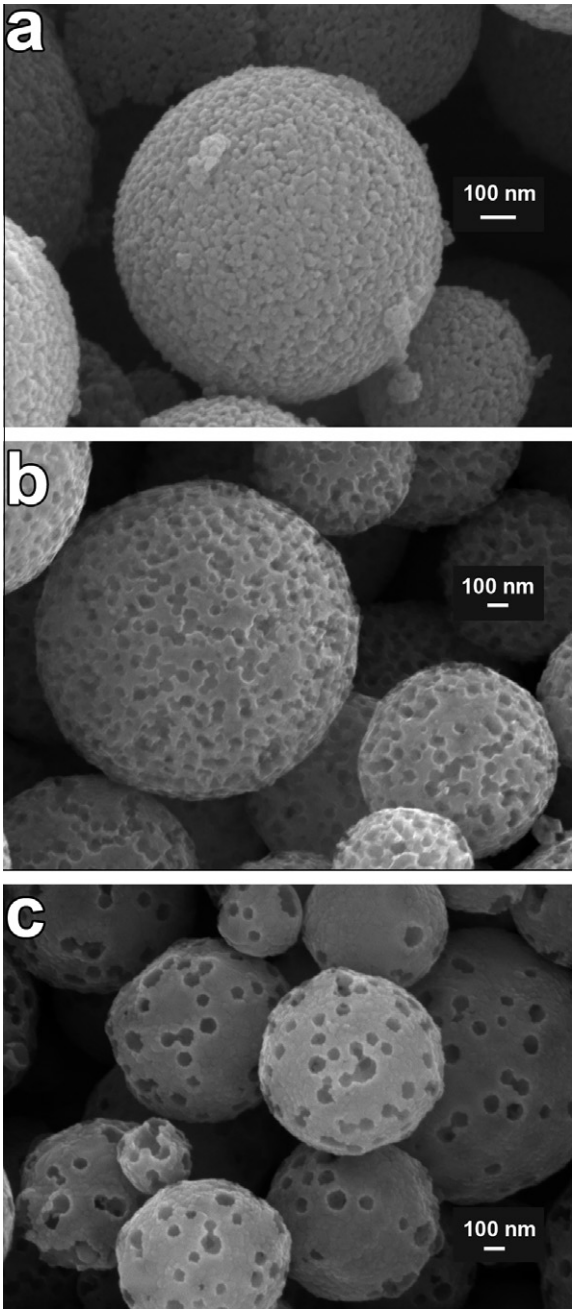

Fig. 3. SEM micrographs showing the effect of silica colloid diameter (d_{Silica}) on the porosity of microspheres obtained with a Si:Ti molar ratio of 1:3. (a) Sample T13S (d_{silica} = 12 nm), (b) T13M (d_{silica} = 35–50 nm), (c) T13L (d_{silica} = 70–100 nm).

nebulizer). Inside the droplets, after water evaporation, a further heating leads to supersaturation, at which point precursor precipitation and decomposition take place [19–23,29–37]. At this stage, the interactions between the hot SiO_2 template particles surface and the TiO_2 precursor become crucial in the material formation process, and especially in the preferential formation of anatase vs. rutile.

TiO_2 is the most common semiconductor used in photocatalytic applications, due to its high oxidation potential, excellent chemical stability, and relatively low cost.

There are three common crystalline forms of TiO_2: rutile, brookite, and anatase. Brookite and anatase are thermodynamically metastable and can be irreversibly transformed to the more stable rutile form at high temperature. The most common source of TiO_2 for photocatalytic studies is P25 titania from Evonik-Degussa, which contains roughly a 3:1 wt. ratio of anatase to rutile. The anatase/rutile interface plays a critical role in enhancing the photogenerated charge carriers lifetime and thus the photocatalytic activity of P25. However, it is well known that the photocatalytic activity of pure anatase is roughly ten-fold more efficient than pure rutile, at least for the photo-degradation of clofibric acid, a lipid regulator drug [59]. There are theoretical suggestions that brookite might be even more photocatalytically efficient [60], but brookite is difficult to obtain in a pure and stable form. Therefore, the control of TiO_2 nanostructures phase composition is an important requirement for obtaining efficient photocatalysts.

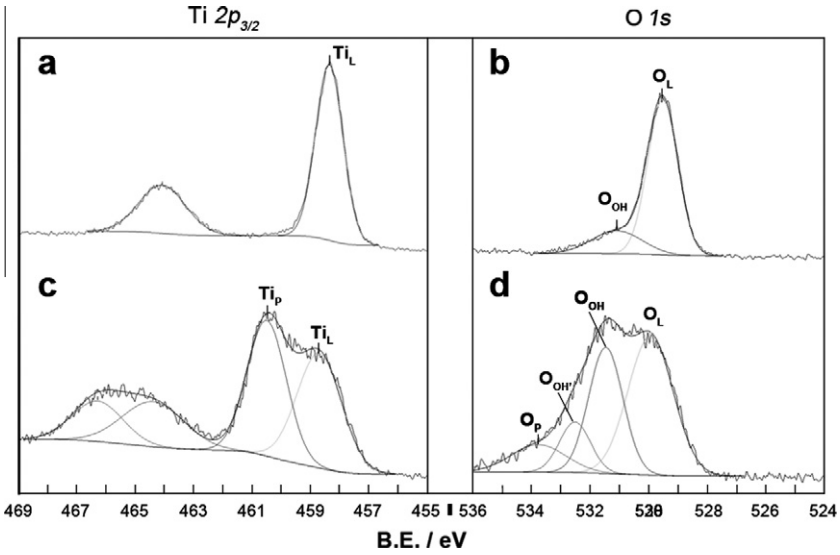

Fig. 4. XPS spectra in the regions for O and Ti: (a and c) a representative porous TiO_2 microsphere (T13S) vs (b and d) the non-porous control (T_USP). The different atomic species present at the surface of the analyzed samples in each spectrum are indicated: Ti_L = lattice titanium; Ti_P = titanium from precursor; O_L = lattice oxygen; O_{OH} = superficial hydroxyl groups; O_P = oxygen from precursor molecules residues; $O_{OH'}$ = superficial hydroxyl related to residue of the precursor molecule.

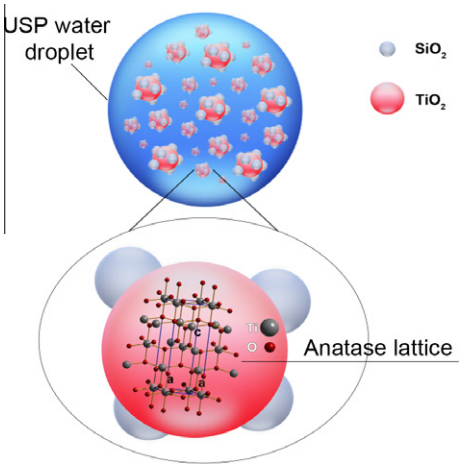

Fig. 5. Schematic illustration of the silica-induced steric hindrance on anatase surfaces (rutile nucleation sites) inside a USP-generated water droplet.

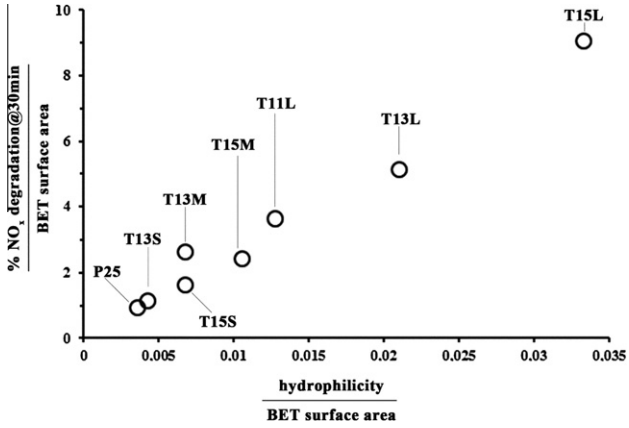

Fig. 6. Chart representing the % NO_x degradation at 30 min normalized by surface area in comparison with the surface hydrophilicity (taken as the XPS-determined surface OH concentrations normalized by the total oxygen atom concentrations, O_{tot}) per unit surface area. The values reported are for Evonik-Degussa P25 titania and for each of the USP-generated porous titania microsphere samples.

We observe a striking increased concentration of anatase relative to rutile phases as a function of increasing silica surface area in the initial formulations (Table 1). As determined from the XRPD (SI, Fig. S3), the solid microspheres produced by USP in the absence of a silica template are only 36% anatase. The porous microspheres, however, have a much greater fraction of anatase, and importantly the anatase fraction increases monotonically with increasing surface area of the added colloidal silica template (Table 1 and plotted in SI, Fig. S4).

Bulk rutile is more stable thermodynamically than anatase at all temperatures and pressures owing to its lower Gibbs free energy However, the lower surface energy of the anatase planes relative to those of rutile causes the former to be more stable in kinetically-regulated process (i.e., USP) [61]. It is well understood that in the anatase to rutile transformation, the Ti–O bonds of the anatase phase structure break and rearrange to form rutile. This process is usually accelerated when defects (i.e., oxygen vacancies) [62], dopants (metal or non-metal) or impurities are present to some extent [61]. In the case of SiO_2-assisted TiO_2 synthesis, SiO_2 precursors (e.g., TEOS) enhanced the phase stability of anatase in batch reactions [63–67]. There are also a few studies of titania growth on silica particles, yielding amorphous TiO_2 coating [68], anatase particles deposition [20], and ion-directed anatase growth.[69–71] Nevertheless, in our USP set-up, colloidal SiO_2 might play a different role. Banfield et al. showed that in dried TiO_2 powder at temperatures higher than 600 °C, both rutile surface nucleation (on anatase particles) and interface nucleation (at the anatase/anatase particles interface) govern the anatase to rutile phase transformation [72]. In the T_USP titania (i.e., in the absence of a silica template), the nanoparticles assembled in the microsphere structure are strongly associated by a high surface contact thus promoting the expected rutile growth. Differently, in the presence of colloidal SiO_2 (Fig. 5), we propose that the SiO_2 surface creates a steric hindrance both for anatase/anatase interfaces and surface sites for rutile nucleation thus decreasing dramatically its formation probability.

The samples' band-gap (Table 1) qualitatively reflected the rutile/anatase ratios found through XRPD data analysis. Diffuse

reflectance data were converted to absorption coefficient values $F(R)$ according to the standard Kubelka–Munk equation (Fig. S5) [73,74]. As expected, the band-gap values so obtained correlate with the anatase content in the samples: the larger the rutile component, the smaller the band gap, which ranges from 2.92 eV for T_USP (36% anatase) to 3.31 eV for T13S (100% anatase). For comparison, titania nanoparticles of rutile and anatase have reported band gaps of 3.00 and 3.21 eV, respectively, whereas thin films of titania on alumina show band gaps of 3.25 and 3.75 eV, respectively [75,76].

In order to test the chemical reactivity of our porous titania microspheres, we examined the photocatalytic activities using gas phase catalytic degradation of NO_x as a probe reaction (cf. Section 2.4 for details) [74]. The porous microspheres showed generally higher activity relative to Evonik-Degussa P25 (SI, Fig. S6); the T11L, T13S, T13 M, T15S, and T15L samples are in fact ≈25% more active after 90 min than P25 on a mass basis and the remainder are comparable to P25.

In terms of photocatalytic activity per surface area (after 30 min), all of the microsphere samples show substantially higher specific activities than P25 with T_USP and T_USP_HF being roughly fifty-fold more active (SI, Table S2).

The increased specific activity per surface area correlates almost linearly with increasing surface hydrophilicity normalized by surface area (Fig. 6 and SI, Table S2). For a quantitative measure of the hydrophilicity of the surface, we used the XPS-determined surface OH atomic concentrations normalized by the total oxygen atom concentrations, O_{tot}: the larger the value of OH/O_{tot} per unit surface area, the higher the observed photocatalytic specific activity per surface area (Fig. 6). Because the non-porous T_USP and T_USP_HF have the most hydrophilic surfaces, they also have the highest specific activity when normalized to surface area (Table S2). We believe that the more hydrophilic titania surfaces adsorb nitrogen oxides (which are small hydrophilic molecules) more effectively at the semiconductor surface, which promotes the photocatalytic reactions resulting in NO_x degradation.

4. Conclusions

In conclusion, we have used ultrasonic spray pyrolysis to prepare porous titania microspheres with tunable porosity and nanostructures and resulting control over their phase composition. We can tailor physical properties of the microspheres' by adjusting both the silica nanoparticle to titanium ratio and the silica particle sizes. Importantly, the silica template suppresses the rutile formation, inducing preferential growth of the anatase phase of titania from pyrolysis of the Ti^{IV} precursor. The adsorption of a hydrophilic pollutant molecule on the TiO_2 surface is crucial for addressing the photocatalytic efficiency, and consistent with that, the porous titania microspheres made by USP show better photocatalytic activity than Evonik-Degussa P25 in the gas phase decomposition of NO_x.

Aknowledgements

We gratefully acknowledge support by the U.S. NSF (DMR 09-06904). Characterizations were carried out in the Center for Microanalysis of Materials, UIUC, which is partially supported by the U.S. DOE under Grants DE-FG02-07ER46453 and DE-FG02-07ER46471.

Appendix A. Supplementary data

Supplementary data associated with this article can be found, in the online version, at http://dx.doi.org/10.1016/j.ultsonch.2012.07.003.

References

[1] R. Lakes, Nature 361 (1993) 511.
[2] F. Caruso, R.A. Caruso, H. Möhwald, Science 282 (1998) 1111.
[3] A. Bigi, E. Boanini, D. Walsh, S. Mann, Angew. Chem. Int. Ed. 41 (2002) 2163.
[4] J. Yang, T. Sasaki, Chem. Mater. 20 (2008) 2049.
[5] H. Zhou, T. Fan, H. Ogawa, Chem. Mater. 19 (2007) 2144.
[6] W.H. Suh, K.S. Suslick, G.D. Stucky, Y.H. Suh, Prog. Neurobiol. 87 (2009) 133.
[7] M.S. Mo, J.C. Yu, L.Z. Zhang, S.-K.A. Li, Adv. Mater. 17 (2005) 756.
[8] A.D. Dinsmore, M.F. Hsu, M. Nikolaides, D.A. Weitz, Science 298 (2002) 1006.
[9] S. Gao, S. Yang, J. Shu, Z. Li, K. Jiang, J. Phys. Chem. C 112 (2008) 19324.
[10] A.M. Cao, J.S. Hu, H.P. Liang, L.J. Wan, Angew. Chem. Int. Ed. 44 (2005) 4391.
[11] B. Fang, J.H. Kim, M. Kim, J.-S. Yu, Phys. Chem. Chem. Phys. 11 (2009) 1380.
[12] Z.W. Shan, G. Adesso, A.P. Alivisatos, Nat. Mater. 7 (2008) 947.
[13] X. Song, L. Gao, J. Phys. Chem. C 12 (2008) 15299.
[14] S.-W. Cao, Y.-J. Zhu, J. Phys. Chem. C 112 (2008) 6253.
[15] J. Fei, Y. Cui, X. Yan, J. Li, Adv. Mater. 20 (2008) 452.
[16] X. Li, Y. Xiong, Y. Xie, Inorg. Chem. 45 (2006) 3493.
[17] H. Li, Z. Bian, Y. Lu, J. Am. Chem. Soc. 129 (2007) 8406.
[18] J. Yu, W. Liu, H. Yu, Cryst. Growth Des. 8 (2008) 930.
[19] X. Song, X. Ding, L. Zhang, J. Phys. Chem. C 113 (2009) 5455.
[20] D. Li, H. Haneda, N. Ohashi, Chem. Mater. 17 (2005) 2588.
[21] W.H. Suh, A.R. Jang, Y.-H. Suh, K.S. Suslick, Adv. Mater. 18 (2006) 1832.
[22] F. Iskandar, A. Nandiyanto, K. Yun, C. Hogan, K. Okuyama, P. Biswas, Adv. Mater. 19 (2007) 1408.
[23] A. Nandiyanto, F. Iskandar, K. Okuyama, Chem. Eng. J. 152 (2009) 293.
[24] C. Yu, J.C. Yu, M. Chan, J. Solid State Chem. 182 (2009) 1061.
[25] W.-G. Yang, F.-R. Wan, Q.-W. Chen, J.-J. Li, D.-S. Xu, J. Mater. Chem. 20 (2010) 2870.
[26] Z. Liu, H. Bai, D. Sun, Appl. Catal. B 104 (2011) 234.
[27] H. Pan, J. Qian, Y. Cui, H. Xie, X. Zhou, J. Mater. Chem. 22 (2012) 6002.
[28] D. Chen, L. Cao, T.L. Hanley, R.A. Caruso, Adv. Funct. Mater. 22 (2012) 1966.
[29] J.H. Bang, K.S. Suslick, Adv. Mater. 22 (2010) 1039.
[30] K. Okuyama, W. Lenggoro, Chem. Eng. Sci. 58 (2003) 537.
[31] P.S. Patil, Mater. Chem. Phys. 59 (1999) 185.
[32] T.T. Kodas, M. Hampden-Smith, Aerosol Processing of Materials, Wiley-VCH, New York, 1999.
[33] G.L. Messing, S.C. Zhang, G.V. Jayanthi, J. Am. Ceram. Soc. 76 (1993) 2707.
[34] M. Ferry Iskandar, K. Okuyama, Nano Lett. 1 (2001) 231.
[35] A. Nandiyanto, S. Kim, F. Iskandar, K. Okuyama, Microporous Mesoporous Mater. 120 (2009) 447.
[36] M. Ferry Iskandar, K. Okuyama, Nano Lett. 2 (2002) 389.
[37] E.K. Athanassiou, R.N. Grass, W.J. Stark, Aerosol Sci. Technol. 44 (2010) 161.
[38] W.H. Suh, K.S. Suslick, J. Am. Chem. Soc. 127 (2005) 12007.
[39] Y.T. Didenko, K.S. Suslick, J. Am. Chem. Soc. 127 (2005) 12196.
[40] S.E. Skrabalak, K.S. Suslick, J. Am. Chem. Soc. 128 (2006) 12642.
[41] J.H. Bang, R.J. Helmich, K.S. Suslick, Adv. Mater. 20 (2008) 2599.
[42] S.S. Dunkle, K.S. Suslick, J. Phys. Chem. C 113 (2009) 10341.
[43] L. Li, C.-K. Tsung, Z. Yang, G.D. Stucky, L.D. Sun, L. Sun, J.F. Wang, C. Yan, Adv. Mater. 20 (2008) 903.
[44] W.-N. Wang, A. Purwanto, I.W. Lenggoro, K. Okuyama, H. Chang, H.D. Jang, Ind. Eng. Chem. Res. 47 (2008) 1650.
[45] H.-D. Jang, H. Chang, K. Cho, S.-J. Kim, J.-H. Park, J.-W. Choi, K. Okuyama, Ultramicroscopy 108 (2008) 1241.
[46] V. Jokanović, A.M. Spasić, D. Uskoković, J. Colloid Interface Sci. 278 (2004) 342.
[47] D. Grosso, G. J. de A.A. Soler-Illia, E.L. Crepaldi, B. Charleux, C. Sanchez, Adv. Funct. Mater. 13 (2003) 37.
[48] S.Y. Lee, L. Gradon, S. Janeczko, F. Iskandar, K. Okuyama, ACS Nano 4 (2010) 4717.
[49] S.K. Kim, H. Chang, K. Cho, D.S. Kil, S.W. Cho, H.D. Jang, J.-W. Choi, J. Choi, Mater. Lett. 65 (2011) 3330.
[50] Y.-H. Tseng, C.-H. Kuo, Catal. Today 174 (2011) 114.
[51] Y. Huang, Y. Wei, J. Wu, C. Guo, M. Wang, S. Yin, T. Sato, Appl. Catal. B 123–124 (2012) 9.
[52] Q. Wu, R. van de Krol, J. Am. Chem. Soc. 134 (2012) 9369.
[53] C.L. Bianchi, G. Cappelletti, S. Ardizzone, S. Gialanella, A. Naldoni, C. Oliva, C. Pirola, Catal. Today 144 (2009) 31.
[54] C.L. Bianchi, C. Pirola, E. Selli, S. Biella, J. Hazard. Mater. 211–212 (2012) 203.
[55] J.F. Moulder, W.F. Stickle, P.E. Solob, K.D. Bombem, Handbook of X-ray Photoelectron Spectroscopy, Physical Electronics, Inc., Eden Prairie, USA, 1995. pp. 221–222.
[56] S. Ardizzone, C.L. Bianchi, G. Cappelletti, A. Naldoni, C. Pirola, Environ. Sci. Technol. 42 (2008) 6671.
[57] Q. Wei, J. Sankar, J. Mater. Res. 15 (2000) 633.
[58] S. Ardizzone, C.L. Bianchi, G. Cappelletti, S. Gialanella, V. Ragaini, J. Phys. Chem. C 111 (2007) 13222.
[59] J.-G. Li, T. Ishigaki, Acta Mater. 52 (2004) 5143.
[60] C.G. Silva, J.L. Faria, Photochem. Photobiol. Sci. 8 (2009) 705.
[61] D.A.H. Hanaor, C.C. Sorrell, J. Mater. Sci. 46 (2011) 855.
[62] M. Salari, K. Konstantinov, H.K. Liu, J. Mater. Chem. 21 (2011) 5128.
[63] M. Yoshinaka, K. Hirota, O. Yamaguchi, J. Am. Ceram. Soc. 80 (1997) 2749.
[64] K. Okada, N. Yamamoto, Y. Kameshima, A. Yasumori, K.J.D.O. MacKenzi, J. Am. Ceram. Soc. 84 (2001) 1591.
[65] H. Kominami, M. Kohno, Y. Matsunaga, Y. Kera, J. Am. Ceram. Soc. 84 (2001) 1178.
[66] C. Anderson, A.J. Bard, J. Phys. Chem. B 101 (1997) 2611.

[67] M. Hirano, K. Ota, H. Iwata, Chem. Mater. 16 (2004) 3725.
[68] A. Hanprasopwattana, S. Srinivasan, A.G. Sault, A.K. Datye, Langmuir 12 (1996) 3173.
[69] W. Yue, C. Randorn, P.S. Attidekou, W. Zhou, Adv. Funct. Mater. 19 (2009) 2826.
[70] S. Vermury, S.E. Pratsinis, J. Am. Ceram. Soc. 78 (1995) 2984.
[71] S. Pratsinis, Prog. Energy Combust. Sci. 24 (1998) 197.
[72] H. Zhang, J.F. Banfield, J. Mater. Res. 15 (2000) 437.
[73] G. Cappelletti, C.L. Bianchi, S. Ardizzone, Appl. Catal. B 78 (2008) 193.
[74] G. Cappelletti, S. Ardizzone, C.L. Bianchi, S. Gialanella, A. Naldoni, C. Pirola, V. Ragaini, Nanoscale Res. Lett. 4 (2009) 97.
[75] D. Reyes-Coronado, G. Rodriguez-Gattorno, M.E. Espinosa-Pesqueira, C. Cab, R. de Coss, G. Oskam, Nanotechnology 19 (2008) 145605.
[76] Y.R. Parka, K.J. Kim, Thin Solid Films 484 (2005) 34.